

SCIENTIFIC REPORTS



OPEN

Supercurrent switch in π topological junctions based upon a narrow quantum spin Hall insulator

Qingyun Yu¹, Ze Tao², Juntao Song³, Y. C. Tao¹ & Jun Wang⁴

The narrow quantum spin Hall (QSH) insulator is characterized by interedge coupling, which could feature exotic transport phenomena, and thus serves as the key element for topological superconducting electronic devices. Herein, we theoretically explore possible Josephson π states in a QSH insulator strip touching on two *s*-wave superconductors in the presence of the interedge coupling. It is shown that the interedge coupling could give rise to a $0 - \pi$ transition modulated by the gate voltage, originating from an additional π phase difference caused by the interedge backscattering. The $0 - \pi$ transition in turn can manifest the helical spin texture of the edge states. A considerable residual value of the supercurrent at the $0 - \pi$ transition point is always exhibited, suggesting a very efficient performance of the device as a supercurrent switch. Moreover, the region of coexisting 0 and π states is found fairly large, which can be used to improve accuracy in the design of a π superconducting quantum interference device.

The quantum spin Hall (QSH) insulator, a kind of two-dimensional topological insulator, is a topologically non-trivial phase of electronic matter^{1–4}. The transport of the QSH insulator is characterized by gapless helical edge states, which are protected by the time reversal symmetry. The spin-up electrons propagate clockwise along the sample edge, while the spin-down do counterclockwise, indicating that the intraedge backscattering is prevented⁵. Therefore, the helical edge states have not only the physical significance but also important applications in topological superconducting spintronics and topological quantum computation^{1–4}. Besides, while the edge-state conduction^{3,4} and the spin polarization of the edge current⁶ have been verified, a direct evidence for the helical spin texture of the edge states remains a challenge⁷. For a narrow QSH insulator with two edges getting close to each other, the overlap between edge states from opposite edges produces an energy gap, leading to the so-called interedge coupling, although the intraedge backscattering is still forbidden⁸. Resultantly, the properties of QSH insulator can be greatly modified and one remarkable property is the elastic interedge backscattering between the edge states at the two sides^{7–9}.

Although a variety of Josephson junctions, on the other hand, have been proposed and observed, so far, the reports on the ones based on narrow QSH insulators lack enough¹⁰. One peculiar feature of some Josephson junctions is the $0 - \pi$ transition^{10–14}, the phase difference ϕ is usually zero in the ground state, however, an extra π phase difference can emerge under appropriate conditions, and so the maximum or critical Josephson current is reversed. The junction with such a π phase difference is called a π junction, or deemed as a supercurrent switch, which can be used as a basic component in superconducting qubits and quantum computing and information^{10–18}. Moreover, the stable and metastable 0 and π states in the crossover coexisting region can yield two flux jumps per one external flux quantum in a superconducting quantum interference device (SQUID)^{19,20}, indicating a potential application in quantum electronics²¹. However, most Josephson junctions generating the $0 - \pi$ transition have their disadvantages. For instance, the one induced by the ferromagnet (FM) exchange energy or the FM layer length of the Josephson junction^{22–24} is not only of difficulty in modulation but also of high-energy in dissipation, being not expected in the quantum qubit application^{16–18}. Hence, it is still highly desirable that a Josephson π junction owns low-energy dissipation and much convenience in manipulation simultaneously. Due

¹Department of Physics and Institute of Theoretical Physics, Nanjing Normal University, Nanjing, 210023, China.

²College of Telecommunications & Information Engineering, Nanjing University of Posts and Telecommunications, Nanjing, 210023, China. ³Department of Physics and Hebei Advanced Thin Film Laboratory, Hebei Normal University, Shijiazhuang, 050024, China. ⁴Department of Physics, Southeast University, Nanjing, 210096, China. Correspondence and requests for materials should be addressed to Y.C.T. (email: yctao88@163.com) or J.W. (email: jwang@seu.edu.cn)

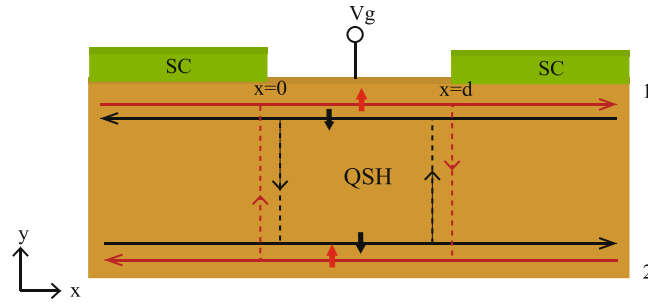


Figure 1. Schematic illustration of the proposed Josephson junction with a gate voltage V_g applied on the middle normal segment of width d . The QSH insulator strip with two edges (edges 1 and 2) is sketched as the orange bar. The red and black lines illustrate the helical edge states with the vertical arrows representing the spin orientation, and the interedge coupling causes interedge backscattering indicated by the dotted lines. The two green bars denote the two s -wave SCs deposited on edge 1.

to the helicity conservation of the carriers, the electron travels in the QSH insulator edge dissipationlessly³⁻⁵, which can be therefore a good candidate for the π junction. Particularly, it is expected to maximize the potential for transport phenomena induced by the interedge backscattering in topological superconducting electronics based on a narrow QSH insulator.

In this letter, we therefore propose a Josephson junction fabricated on the narrow QSH insulator strip with the longitudinal direction along the x axis as shown in Fig. 1, where two s -wave superconductors (SCs) are in intimate contact with one edge of the strip (edge 1)²⁵ and the middle normal segment sandwiched between them is applied by a gate voltage V_g . Compared with the interedge coupling strength $\alpha(x)$ in the middle region ($0 < x < d$) assumed to be α_2 , a lower one α_1 exhibits in the left and right regions, stemming from that the wave functions of electrons in the QSH insulator strip can penetrate into the bulk SC²⁶. Due to the proximity effect, a superconducting pair potential is induced in the contacting areas^{25,27}, and its amplitude depends upon the coupling between the edge and the SC. Only edge 1 in touch with the SC can be assumed superconducting while edge 2 keeps normal thanks to the superconducting gap penetrating into the QSH insulator with only a few atomic layers²⁸. In the proposed setup, owing to the interedge backscattering, a $0 - \pi$ transition is found to be manipulated by the gate voltage V_g , which embodies the helical spin texture of the edge states in the QSH insulator. It is also shown that there exists not only a fairly large residual value of critical Josephson current at the $0 - \pi$ transition point but also a large region of coexisting 0 and π states. The results pave the way toward the designs of a low-energy dissipation supercurrent switch with high efficiency and a π SQUID with improved accuracy.

Topological Josephson junctions with interedge coupling. Due to the edge states in the QSH insulator strip protected by the time reversal symmetry, no spin-flip effects are assumed²⁹. Hence, we can apply the four-spinor wave function $\Psi_\sigma(x) = (u_{1\sigma}(x), u_{2\sigma}(x), v_{1\bar{\sigma}}(x), v_{2\bar{\sigma}}(x))^T$ for this system, where σ denotes the spin orientation ($\sigma = \uparrow, \downarrow$), $\bar{\sigma}$ is opposite to σ , the wave functions $u_{1(2)}$ and $v_{1(2)}$ stand for the probability amplitudes of the electron and hole in edge 1(2), respectively. The Bogoliubov-de Gennes (BdG) equation³⁰ is given by

$$H_{BdG}\Psi_\sigma(x) = E\Psi_\sigma(x) \tag{1}$$

with E the quasiparticle energy measured from the Fermi energy E_F and ref. 29

$$H_{BdG} = \begin{pmatrix} h_{1\sigma} & \alpha(x) & \Delta(x) & 0 \\ \alpha(x) & h_{2\sigma} & 0 & 0 \\ \Delta^*(x) & 0 & -h_{1\sigma} & -\alpha(x) \\ 0 & 0 & -\alpha(x) & -h_{2\sigma} \end{pmatrix},$$

where $h_{1(2)\sigma} = \mp i\hbar v_F \partial_x - \mu(x)$ is the Dirac-like Hamiltonian for helical particles in the two edges with the Fermi velocity v_F , the chemical potential $\mu(x)$, and the positive (negative) sign for spin-down (spin-up) electrons in edge 1 and spin-up (spin-down) electrons in edge 2. $\mu(x)$ is assumed 0 for the two superconducting regions and is controlled by a gate voltage V_g for the middle region. The superconducting pair potential $\Delta(x) = \Delta e^{i\phi_{L(R)}}$ for the left (right) superconducting region exists only in edge 1 with $\phi_{L(R)}$ the superconducting phase, while $\Delta(x) = 0$ for the middle. The temperature dependence of Δ is given by $\Delta \equiv \Delta(T) = \Delta_0 \tanh(1.74\sqrt{T_c/T - 1})$. The macroscopic phase difference across the junction is defined as $\phi = \phi_R - \phi_L$.

For the injection of an electron-like quasiparticle (ELQ) with energy $E > \Delta$ from the left SC region, with the general solution of Eq. (1), the wave function in the left s -wave SC region is given by

$$\Psi_L(x) = \psi_{L+}^e + b_1\psi_{L-}^e + a_1\psi_{L-}^h \tag{2}$$

for $x < 0$, where $\psi_{L\pm}^e = \{\eta^\pm(E \pm \hbar v_F k^e)/\alpha_1, \eta^\pm, \eta^\pm \lambda e^{-i\phi_L}/(\alpha_1 \Delta), -\eta^\pm \lambda e^{-i\phi_L}/[(E \mp \hbar v_F k^e) \Delta]\}^T e^{\pm ik^e x}$ with $\lambda = E^2 - (\hbar v_F k^e)^2 - \alpha_1^2$ and $\eta^\pm = \sqrt{[(E \pm \hbar v_F k^e)/\alpha_1]^2 + 1 + |\lambda/(\alpha_1 \Delta)|^2 + |\lambda|[(E \mp \hbar v_F k^e) \Delta]}^2}$, and $\psi_{L\pm}^h =$

$\{\gamma^\pm(E \pm \hbar v_F k^h)/\alpha_1, \gamma^\pm, \gamma^\pm \nu e^{-i\phi_L}/(\alpha_1 \Delta), -\gamma^\pm \nu e^{-i\phi_L}/[(E \mp \hbar v_F k^h) \Delta]\}^T e^{\pm ik^h x}$ with $\gamma^\pm = \sqrt{|(E \pm \hbar v_F k^h)/\alpha_1|^2 + \sqrt{1 + |\nu/(\alpha_1 \Delta)|^2 + |\nu/[(E \mp \hbar v_F k^h) \Delta]|^2}}$ and $\nu = E^2 - (\hbar v_F k^h)^2 - \alpha_1^2$. The wave vectors in the SC regions are given by $k^{e(h)} = \sqrt{E^2 - \alpha_1^2 - \frac{1}{2}\Delta(\Delta + (-)\sqrt{\Delta^2 + 4\alpha_1^2})}/(\hbar v_F)$. The coefficients a_1 and b_1 are, respectively, the amplitudes of the Andreev reflection (AR) as a hole-like quasiparticle (HLQ), and normal reflection as an ELQ. In the middle region, we have the wave function

$$\Psi_M(x) = g_1 \psi_1 + g_2 \psi_2 + g_3 \psi_3 + g_4 \psi_4 \quad (3)$$

for $0 < x < d$, where $\psi_1 = [\cos(\theta/2), \sin(\theta/2), 0, 0]^T e^{iq^e x}$ with $\sin \theta = \alpha_2/(E - V_g)$, $\psi_2 = [\sin(\theta/2), \cos(\theta/2), 0, 0]^T e^{-iq^e x}$, $\psi_3 = [0, 0, -\sin(\varphi/2), \cos(\varphi/2)]^T e^{iq^h x}$ with $\sin \varphi = \alpha_2/(E + V_g)$, and $\psi_4 = [0, 0, -\cos(\varphi/2), \sin(\varphi/2)]^T e^{-iq^h x}$. The wave vectors in the middle region are given by $q^{e(h)} = \sqrt{(E - (+)V_g)^2 - \alpha_2^2}/(\hbar v_F)$. Amplitudes of electrons and holes propagating in the middle region are given by the coefficients $g_i (i = 1 - 4)$. The wave function in the right s -wave SC region is given by

$$\Psi_R(x) = c_1 \psi_{R+}^e + d_1 \psi_{R+}^h \quad (4)$$

for $x > d$, where coefficients c_1 and d_1 are, respectively, the amplitudes of the transmission to the right SC as an ELQ, and transmission to the right SC as a HLQ. $\psi_{R\pm}^e$ and $\psi_{R\pm}^h$ can be respectively obtained from $\psi_{L\pm}^e$ and $\psi_{L\pm}^h$ by making an exchange between L and R .

All the coefficients a_1, b_1, c_1, d_1 , and g_i will be determined by matching the boundary conditions

$$\Psi_L(x)|_{x=0_-} = \Psi_M(x)|_{x=0_+}, \quad \Psi_M(x)|_{x=d_-} = \Psi_R(x)|_{x=d_+}. \quad (5)$$

Analogously, one can easily obtain the AR amplitude a_2 for the injection of a HLQ with energy $E > \Delta$ from the left SC region. The analytical expressions for a_1 and a_2 , are respectively given by

$$a_1 = A_1 + (A_2 e^{i\phi} + A_3 e^{i\zeta^+} + A_4 e^{-i\zeta^+} + A_5 e^{i\zeta^-} + A_6 e^{-i\zeta^-})/G \quad (6)$$

and

$$a_2 = B_1 - (B_2 e^{i\phi} + B_3 e^{i\zeta^+} + B_4 e^{-i\zeta^+} + B_5 e^{i\zeta^-} + B_6 e^{-i\zeta^-})/G \quad (7)$$

with $G = C_1 e^{i\phi} + C_2 e^{-i\phi} + C_3 e^{i\zeta^+} + C_4 e^{-i\zeta^+} + C_5 e^{i\zeta^-} + C_6 e^{-i\zeta^-}$, where $\zeta^\pm = d(q^e \pm q^h)$ characterize physically important oscillations of the AR amplitudes $a_{1(2)}$, $A_i (i = 1-6)$, $B_i (i = 1-6)$, and $C_i (i = 1-6)$ are complex functions of E, Δ, V_g, α_1 , and α_2 . Then, the dc Josephson current at a given temperature can be expressed in terms of the AR amplitudes a_1 and a_2 by using the temperature Green's function formalism³¹

$$I(\phi) = \frac{e\Delta}{4\hbar} k_B T \sum_{\omega_n, \sigma} \frac{1}{\Omega_n} (k_n^e + k_n^h) \left(\frac{a_{1n}^e}{k_n^e} - \frac{a_{2n}^h}{k_n^h} \right), \quad (8)$$

where k_n^e, k_n^h, a_{1n} , and a_{2n} are respectively obtained from k^e, k^h, a_1 , and a_2 by the analytic continuation $E \rightarrow i\omega_n$. The Matsubara frequencies are $\omega_n = \pi k_B T (2n + 1)$ with $n = 0, \pm 1, \pm 2, \dots$, and $\Omega_n = \sqrt{\omega_n^2 + \Delta^2}$.

The dc Josephson current can be acquired by another formalism^{11, 32-34} $I = \frac{2e}{\hbar} \sum_i \frac{dE_i(\phi)}{d\phi} f(E_i)$ with $f(E_i)$ the Fermi-Dirac distribution and $E_i(\phi) = \pm E(\phi)$ the two energies for a single pair of Andreev bound states which can be arrived at from the BdG equation. Here, each Andreev bound state carries a current and the \pm denotes two possible processes, which differ in direction of propagation of the electrons and holes and correspond to the currents following in opposite directions. In fact, the terms $\frac{dE_i(\phi)}{d\phi}$ are just corresponding to the ARs terms a_1 and a_2 in Eq. (8), so the two methods are equivalent.

A0 - π transition induced by interedge backscattering. In the following calculations, the critical or maximum Josephson current, the relevant quantity measured experimentally²²⁻²⁴, is defined as $I_c = |\max\{I(\phi)\}|$ with the unit of Josephson current¹⁵ $I_0 = 2e\Delta_0/\hbar$. We have taken the units $\hbar v_F = 1$ and $\Delta_0 = 1$ and set the temperature $T = 0.1T_c$, where the critical temperature $T_c \approx 0.57\Delta_0/k_B$ based on the BCS theory.

On the basis of Eq. (8), we calculate the critical Josephson current I_c as a function of gate voltage V_g for different interedge coupling strengths α_2 , which is illustrated in Fig. 2(a). I_c is shown to oscillate with V_g but decay weakly and has three peaks and three dips. This can be explained by two additional phase factors ζ^\pm in analytical expressions $a_{1(2)}$ modulated by V_g . The dips in I_c correspond to the $0 - \pi$ or $\pi - 0$ transition that can be easily controlled by V_g and thus is very useful for applications. Moreover, the positions of both the first and third dips are found to shift toward the smaller V_g with increasing α_2 , however, the position of the second dip toward the bigger V_g . In particular, the value for each dip is decreased with the enhancement of α_2 , implying that α_2 can suppress the Josephson current. Most interestingly, we find that there are considerable residual values of I_c at the dips, which should be experimentally detectable, as in ref. 15. For comparison, I_c as a function of V_g without interedge coupling is also presented in the inset of Fig. 2(a). With V_g increased, I_c remains constant, indicating no

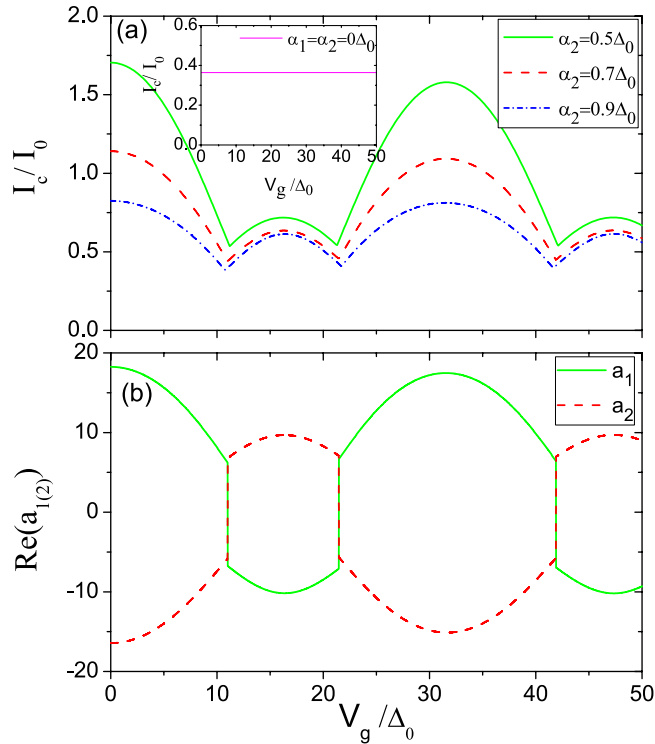


Figure 2. (a) The critical Josephson current I_c as a function of gate voltage V_g for different interedge coupling strengths α_2 . The inset shows I_c as a function of V_g without interedge coupling. (b) Andreev reflection coefficients a_1 and a_2 as a function of V_g , corresponding to the red dashed line in Fig. 2(a), coming from the contribution of all channels. Here, $\alpha_1 = 0.5\alpha_2$, $d = 0.1\xi_0$ with $\xi_0 = \hbar v_F/\Delta_0$ superconducting coherence length at zero temperature, and the various α_2 are indicated.

$0 - \pi$ transition as demonstrated theoretically in refs 34 and 35. This is physically natural as in s -wave SC/normal metal/ s -wave SC structure.

In order to understand how the AR amplitudes $a_{1(2)}$ for the incident ELQ (HLQ) determine the $0 - \pi$ transition under the interedge coupling, we present in Fig. 2(b), the AR amplitudes a_1 and a_2 as a function of gate voltage V_g at $\alpha_2 = 0.7\Delta_0$ including the contribution from all channels, corresponding to the red dashed line in Fig. 2(a). With increasing V_g , a_1 first decreases from positive value, then abruptly jumps to the negative value at the gate voltage $V_g \equiv V_{g(c)} = 11\Delta_0$, namely at the first dip, however, although the situation for a_2 is just contrary, the currents carried by the two ARs are of the same direction and the magnitudes of a_1 and a_2 are slightly different. At the voltage value $V_{g(c)}$, the critical Josephson currents I_c for the positive and negative directions are equal, which respectively correspond to the two different phase differences as detailed in Fig. 3, thus a $0 - \pi$ transition from the positive to negative direction for the I_c takes place. With the further increase of V_g , $a_{1(2)}$ becomes positive (negative) again at the second dip, then turns negative (positive) again at the third dip, where the former and latter are respectively corresponding to $\pi - 0$ and $0 - \pi$ transitions.

Physically, the $0 - \pi$ transition in SC/FM/SC junction is attributed to the tunneling Cooper pair acquiring a nonzero momentum due to FM exchange splitting in the FM region. However, in the present structure, compared with the case of no interedge coupling, since there is no difference between the spin-up and -down electrons, the $0 - \pi$ transition tuned by the gate voltage V_g should be just originated from the interedge coupling, which induces an additional π phase difference in $I(\phi)$. Specifically, in the context of the interedge coupling, the interedge backscattering between the edge states at two sides can occur at the interface between the left (right) and middle regions, but the intraedge backscattering is still prevented on account of the helical nature of the edge states⁷⁻⁹. The wave from the AR at interface $x=0$ in edge 1 and that from the interedge backscattering at the interface in edge 2 are destructively coherent, leading to the additional π phase difference and the resultant $0 - \pi$ transition modulated by V_g . The additional π phase difference can be also seen from the two ARs $a_{1(2)}$ varying with V_g under the interedge coupling, as shown in Fig. 2(b). The physical mechanism of $0 - \pi$ transition by V_g stemming from the interedge coupling can be described as follows. With increasing V_g , the mismatch from the quasiparticle wave in the middle region, which can be effectively regarded as a barrier at the interface, gets large. It follows that the AR is suppressed, whereas the normal reflection is stimulated. Particularly, due to the interedge coupling, the fraction of the former in edge 2 is strongly inhibited and that of the latter is largely enhanced. As their competition reaches to a certain degree, the direction of the current in edge 2 is reversed. As a result, the supercurrent in edge 1 also exhibits sign reversal with it, thus the AR $a_{1(2)}$ jumps from the positive (negative) to negative (positive) value and a dip of I_c with V_g emerges, resulting in a $0 - \pi$ transition. The same mechanism is for the subsequent $\pi - 0$ and $0 - \pi$ transitions. Furthermore, the $0 - \pi$ transition tuned by V_g in turn can demonstrate the helical spin texture of the edge states.

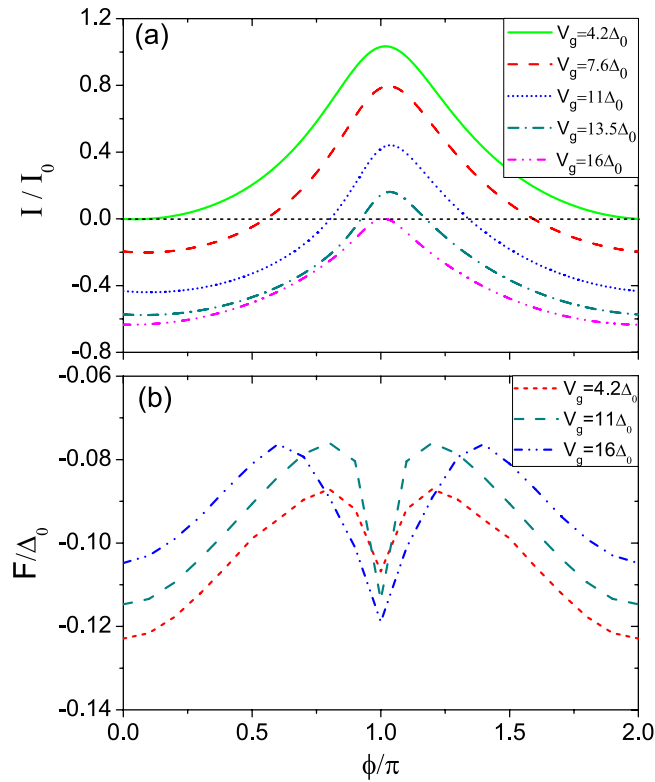


Figure 3. (a) Current-phase relations $I(\phi)$ with various V_g corresponding to the first dip of red dashed line in Fig. 2(a). Here, the parameters are the same as those as in Fig. 2 except that $\alpha_2 = 0.7\Delta_0$ and the various V_g are indicated. (b) The ϕ dependences of the free energy F in the junction at the crossover point ($V_{g(c)} = 11\Delta_0$), 0-state ($V_g = 4.2\Delta_0$), and π -state ($V_g = 16\Delta_0$).

Next, the characteristic variations of the highly nonsinusoidal current-phase relation $I(\phi)$ in the vicinity of the crossover between 0 and π states, for instance, corresponding to the first dip of red dashed line in Fig. 2(a), is plotted at different V_g with $\alpha_2 = 0.7\Delta_0$ in Fig. 3(a). It is seen that with the enhancement of V_g , the junction will evolve from the normal 0 state ($V_g = 4.2\Delta_0$) to the abnormal π one ($V_g = 16\Delta_0$) with the magnitude of the gate voltage of the corresponding dip $V_{g(c)} = 11\Delta_0$. The lines in Fig. 3(a) typically show that the critical Josephson current I_c could be reversed with suitable parameters, and a π state could form in the system. I_c for the 0 state corresponds to ϕ being around π , while that for the π state is at $\phi = 0$, which is different from the situation for the conventional 0 – π transition. At the crossover point, I_c for the 0 state is equal to that for the π state, as has been mentioned above. Tracking the absolute value of the current with increasing V_g from Fig. 3(a), one finds that I_c never becomes zero and has a large residual value at the 0 – π transition point. In addition, the region of coexisting 0 and π states is considerably large, which can be employed, e.g., in the design of a π SQUID with improved accuracy, a typical device with an effectively two times smaller flux quantum^{19,20}. To show more clearly that the 0- and π -states are just the ones whose corresponding ϕ are respectively 0 and π , we present the ϕ dependences of the free energy F in the junction at the crossover point ($V_{g(c)} = 11\Delta_0$), 0-state ($V_g = 4.2\Delta_0$), and π -state ($V_g = 16\Delta_0$), as illustrated by Fig. 3(b). It is demonstrated the minimum of the F in the two states is actually located at $\phi = 0$ and $\phi = \pi$, respectively, not only the crossover point, indicating that the junction really owns the 0- and π -states as in usual metallic SC/FM/SC junctions of refs 11–13, and thus can be possibly applied to a qubit or SQUID. The relation between the $I(\phi)$ and F is of slight novelty and a little different from that of usual situation, just originating from the interedge coupling inducing the 0 – π transition.

Experimental feasibility. We now discuss the feasibility of experiments using the QSH insulator in HgTe/CdTe quantum wells³⁶. It was reported that with the separation between edge channels equaling to 400 nm³⁶, the interedge coupling strength α_2 was estimated to be about 10 μeV ⁸. This interedge coupling strength is of the same order as the proximity-induced superconducting gap in the edge states with the maximum value of Δ_0 estimated by 20 μeV for Ti/Al superconducting material³⁶, meaning that the interedge coupling strength in our calculation is experimentally achievable. Furthermore, the bulk band gap of the HgTe/CdTe quantum well is typically $E_g \sim 1 - 30 \text{ meV}$ ^{3,4} and the gate voltage V_g in our calculation is from 0 to $50\Delta_0$, i.e., $V_g \leq 1 \text{ meV}$, therefore, the requirement of the transport at the Fermi energy inside the bulk gap can also be satisfied. The thermal activation $k_B T \approx 0.057\Delta_0$ at the fixed temperature $T = 0.1T_c$, reaching a maximum of 1.14 μeV , is much less than the bulk band gap as well. The gate voltage of around $10\Delta_0 \sim 0.2 \text{ meV}$ can be acceptable for qubit or SQUID application, which is addressed in what follows. Although the present π junction in this work can be considered metallic, being a little similar to the π SC/FM/SC junction of ref. 18, it is characterized by gapless helical edge states and

is quasi one-dimensional for the flow of the supercurrent. The expected heat generation by $V_g \sim 0.2$ meV is estimated to be $0.04\Delta_0$, being smaller than the thermal activation $k_B T$, are distributed on edges 1 and 2, therefore the consequent effect can be greatly reduced, especially after long decoherence time or even by applying a dilution refrigerator as usual in ref. 37. Also, the expected heat generation by V_g is found to be tuned by the interedge coupling. It is demonstrated from our calculation that the Andreev bound state energy in the present π junction is always smaller than $0.5\Delta_0$, but is not too small. And hence, if the present π junction and a 0 junction constitute a superconducting qubit as in ref. 18, the present metallic π junction is also well gapped in energy gap of two-level quantum state for the qubit where the quantum tunneling occurs. This implies that the quasiparticle tunneling which can cause the dissipation is also strongly suppressed at low temperatures. Though the heat generation may be of influence on the two-level quantum state of the qubit, thus leading to the slight shortening of decoherence time, it is a lot less than the energy gap between the two-level quantum states, which can be the same order in magnitude as that in ref. 18. In other words, the heat generation would be strongly overwhelmed by the energy gap, meaning no significant effect on the decoherence time. In particular, if manipulating the interedge coupling appropriately, one can not only prolong the decoherence time adequately but also reduce the heat generation fully.

In summary, we have proposed one setup for Josephson effect based on a narrow QSH insulator strip, which is shown to reveal an obvious $0 - \pi$ transition tuned by gate voltage due to the interedge backscattering. It is also demonstrated that the setup has three advantages: (1) the helical particles travel in the QSH insulator edge dissipationlessly due to the helicity conservation of the carriers, (2) the critical Josephson current I_c at the $0 - \pi$ transition point has a considerable residual value, and (3) the region of coexisting 0 and π states is found fairly large. The setup can be therefore used to design the low-energy dissipation supercurrent switch with high efficiency and a π SQUID with improved accuracy. The devices are likely to be achieved in mercury quantum wells and also provide an evidence of the helical spin texture of the edge states in the QSH insulator.

References

- Hasan, M. Z. & Kane, C. L. Colloquium: Topological insulators. *Rev. Mod. Phys.* **82**, 3045–3067 (2010).
- Qi, X. L. & Zhang, S. C. Topological insulators and superconductors. *Rev. Mod. Phys.* **83**, 1057–1110 (2011).
- König, M. *et al.* Quantum Spin Hall Insulator State in HgTe Quantum Wells. *Science* **318**, 766–770 (2007).
- Roth, A. *et al.* Nonlocal Transport in the Quantum Spin Hall State. *Science* **325**, 294–297 (2009).
- Wu, C., Bernevig, B. A. & Zhang, S. C. Helical Liquid and the Edge of Quantum Spin Hall Systems. *Phys. Rev. Lett.* **96**, 106401-1–106401-4 (2006).
- Brüne, C. *et al.* Spin polarization of the quantum spin Hall edge states. *Nat. Phys.* **8**, 485–490 (2012).
- Chen, W. *et al.* π Spin Berry Phase in a Quantum-Spin-Hall-Insulator-Based Interferometer: Evidence for the Helical Spin Texture of the Edge States. *Phys. Rev. Lett.* **117**, 076802-1–076802-6 (2016).
- Zhou, B., Lu, H. Z., Chu, R. L., Shen, S. Q. & Niu, Q. Finite Size Effects on Helical Edge States in a Quantum Spin-Hall System. *Phys. Rev. Lett.* **101**, 246807-1–246807-4 (2008).
- Li, W., Zang, J. D. & Jiang, Y. J. Size effects on transport properties in topological Anderson insulators. *Phys. Rev. B* **84**, 033409-1–033409-4 (2011).
- Zyuzin, A., Alidoust, M., Klinovaja, J. & Loss, D. Supercurrent reversal in two-dimensional topological insulators. *Phys. Rev. B* **92**, 174515-1–174515-6 (2015).
- Golubov, A. A., Kupriyanov, M. Y. & Il'ichev, E. The current-phase relation in Josephson junctions. *Rev. Mod. Phys.* **76**, 411–469 (2004).
- Buzdin, A. I. Proximity effects in superconductor-ferromagnet heterostructures. *Rev. Mod. Phys.* **77**, 935–976 (2005).
- Bergeret, F. S., Volkov, A. F. & Efetov, K. B. Odd triplet superconductivity and related phenomena in superconductor-ferromagnet structures. *Rev. Mod. Phys.* **77**, 1321–1373 (2005).
- Zyuzin, A., Alidoust, M. & Loss, D. Josephson junction through a disordered topological insulator with helical magnetization. *Phys. Rev. B* **93**, 214502-1–214502-9 (2016).
- Linder, J., Yokoyama, T., Huertas-Hernando, D. & Sudbø, A. Supercurrent Switch in Graphene π Junctions. *Phys. Rev. Lett.* **100**, 187004-1–187004-4 (2008).
- Wang, J., Yang, Y. H. & Chan, K. S. Josephson π state induced by valley polarization. *Phys. Rev. B* **89**, 064501-1–064501-5 (2014).
- Ioffe, L. B. *et al.* Environmentally decoupled *sds*-wave Josephson junctions for quantum computing. *Nature* **398**, 679–681 (1999).
- Yamashita, T., Tanikawa, K., Takahashi, S. & Maekawa, S. Superconducting π Qubit with a Ferromagnetic Josephson junction. *Phys. Rev. Lett.* **95**, 097001-1–097001-4 (2005).
- Radović, Z., Dobrosavljević-Grujić, L. & Vujčić, B. Coexistence of stable and metastable 0 and π states in Josephson junctions. *Phys. Rev. B* **63**, 214512-1–214512-6 (2001).
- Radović, Z., Lazarides, N. & Flytzanis, N. Josephson effect in double-barrier superconductor-ferromagnet junctions. *Phys. Rev. B* **68**, 014501-1–014501-8 (2003).
- Blatter, G., Geshkenbein, V. B. & Ioffe, L. B. Design aspects of superconducting-phase quantum bits. *Phys. Rev. B* **63**, 174511-1–174511-9 (2001).
- Ryazanov, V. V. *et al.* Coupling of Two Superconductors through a Ferromagnet: Evidence for a π Junction. *Phys. Rev. Lett.* **86**, 2427–2430 (2001).
- Kontos, T. *et al.* Josephson Junction through a Thin Ferromagnetic Layer: Negative Coupling. *Phys. Rev. Lett.* **89**, 137007-1–137007-4 (2002).
- Blum, Y., Tsukernik, A., Karpovski, M. & Palevski, A. Oscillations of the Superconducting Critical Current in Nb-Cu-Ni-Cu-Nb Junctions. *Phys. Rev. Lett.* **89**, 187004-1–187004-4 (2002).
- Adroguer, P. *et al.* Probing the helical edge states of a topological insulator by Cooper-pair injection. *Phys. Rev. B* **82**, 081303-1–081303-4 (2010).
- Stanescu, T. D., Sau, J. D., Lutchyn, R. M. & Das Sarma, S. Proximity effect at the superconductor-topological insulator interface. *Phys. Rev. B* **81**, 241310-1–241310-4 (2010).
- Fu, L. & Kane, C. L. Superconducting Proximity Effect and Majorana Fermions at the Surface of a Topological Insulator. *Phys. Rev. Lett.* **100**, 096407-1–096407-4 (2008).
- Black-Schaffer, A. M. Self-consistent superconducting proximity effect at the quantum spin Hall edge. *Phys. Rev. B* **83**, 060504-1–060504-4 (2011).
- Chen, W., Shen, R., Sheng, L., Wang, B. G. & Xing, D. Y. Resonant nonlocal Andreev reflection in a narrow quantum spin Hall system. *Phys. Rev. B* **84**, 115420-1–115420-6 (2011).
- Gennes, P. G. D. *Superconductivity of Metals and Alloys* (Benjamin, New York, 1966).
- Furusaki, A. & Tsukada, M. *Solid State Commun.* **78**, 299 (1991).

32. Beenakker, C. W. J. Universal Limit of Critical-Current Fluctuations in Mesoscopic Josephson Junctions. *Phys. Rev. Lett.* **67**, 3836–3839 (1991).
33. Bagwell, P. F. Suppression of the Josephson current through a narrow, mesoscopic, semiconductor channel by a single impurity. *Phys. Rev. B* **46**, 12573–12586 (1992).
34. Olund, C. T. & Zhao, E. Current-phase relation for Josephson effect through helical metal. *Phys. Rev. B* **86**, 214515-1–214515-7 (2012).
35. Tkachov, G. & Hankiewicz, E. M. Helical Andreev bound states and superconducting Klein tunneling in topological insulator Josephson junctions. *Phys. Rev. B* **88**, 075401-1–075401-8 (2013).
36. Hart, S. *et al.* Induced superconductivity in the quantum spin Hall edge. *Nat. Phys.* **10**, 638–643 (2014).
37. Yang, Yu *et al.* Energy Relaxation Time between Macroscopic Quantum Levels in a Superconducting Persistent-Current Qubit. *Phys. Rev. Lett.* **92**, 117904-1–117904-4 (2004).

Acknowledgements

This work was supported by the National Science Foundation of China under Grant Nos 10947005, 10974170, and 110704032, the Natural Science Foundation of Jiangsu Province under Grant No. BK2009399, and the Natural Science Foundation of Jiangsu Education Department of China under Grant No. 2008102TSJ0083, the Innovation Project for graduate students of Jiangsu Province Higher Education Institutions under Grant No. KYLX16_1266, the Innovation Project for college students of Nanjing University of Posts and Telecommunications under Grant No. XYB2017017.

Author Contributions

Y.C.T. conceived the work, Q.Y.Y. performed the analytical and numerical calculations, Q.Y.Y., Z.T., Y.C.T., J.T.S. and J.W. wrote the manuscript. All authors discussed the results and reviewed the manuscript.

Additional Information

Competing Interests: The authors declare that they have no competing interests.

Publisher's note: Springer Nature remains neutral with regard to jurisdictional claims in published maps and institutional affiliations.



Open Access This article is licensed under a Creative Commons Attribution 4.0 International License, which permits use, sharing, adaptation, distribution and reproduction in any medium or format, as long as you give appropriate credit to the original author(s) and the source, provide a link to the Creative Commons license, and indicate if changes were made. The images or other third party material in this article are included in the article's Creative Commons license, unless indicated otherwise in a credit line to the material. If material is not included in the article's Creative Commons license and your intended use is not permitted by statutory regulation or exceeds the permitted use, you will need to obtain permission directly from the copyright holder. To view a copy of this license, visit <http://creativecommons.org/licenses/by/4.0/>.

© The Author(s) 2017